Research Article

Kholoud Saad Albalawi, Ashish Kumar*, Badr Saad Alqahtani, and Pranay Goswami

Numerical solution of general order Emden-Fowler-type Pantograph delay differential equations

https://doi.org/10.1515/dema-2024-0023
received November 28, 2023; accepted May 11, 2024

Abstract: The present study introduces the Haar wavelet method, which utilizes collocation points to approximate solutions to the Emden-Fowler Pantograph delay differential equations (PDDEs) of general order. This semi-analytic method requires the transformation of the original differential equation into a system of nonlinear differential equations, which is then solved to determine the Haar coefficients. The method's application to fourth-, fifth-, and sixth-order PDDEs is discussed, along with an examination of convergence that involves the determination of an upper bound and the formulation of the rate of convergence for the method. Numerical simulations and error tables are presented to demonstrate the effectiveness and precision of this approach. The error tables clearly illustrate that the method's accuracy improves progressively with increasing resolution.

Keywords: Pantograph delay differential equations, Emden-Fowler-type equations, Haar wavelet method

MSC 2020: Primary 34A34, 65L60, 65T60

1 Introduction and mathematical preliminaries

The Emden-Fowler equations, named after their respective contributors, Emden [1] and Fowler [2], are a set of nonlinear differential equations that arise in astrophysics and other areas of physics, especially when examining the composition of stars [3,4] and the behavior of polytropic gases [5]. The Emden-Fowler equations can be solved numerically to determine the radial distribution of the density, pressure, temperature, and other physical quantities within the star. The Emden-Fowler equation can be expressed in the following general form:

$$v^{-\xi}\frac{\mathrm{d}^{\varepsilon_1}}{\mathrm{d}v^{\varepsilon_1}}\left(v^{\xi}\frac{\mathrm{d}^{\varepsilon_2}}{\mathrm{d}v^{\varepsilon_2}}\right)w + s(v)g(w) = 0, \tag{1}$$

where $s(v)$ is a nonlinear function, $\varepsilon_1 + \varepsilon_2$ gives the order of the equation.

Astrophysical fluid dynamics [6] is a field of study that deals with the behavior of fluids in the presence of gravity. It is a complex subject, and one way to model these behaviors [7] is through the use of Emden-Fowler equations. These equations are particularly useful when it comes to dealing with scenarios that involve polytropic equations of state. In such scenarios, the Emden-Fowler equations can be used as a tool for

* **Corresponding author: Ashish Kumar**, School of Liberal Studies, Dr B. R. Ambedkar University Delhi, Delhi-110006, India, e-mail: ashish4747.ak@gmail.com
Kholoud Saad Albalawi: Department of Mathematics and Statistics, College of Science, Imam Mohammad Ibn Saud Islamic University, Riyadh 11566, Saudi Arabia, e-mail: Ksalbalawi@imamu.edu.sa
Badr Saad Alqahtani: Department of Mathematics, College of Science, King Saud University, Riyadh 11989, Saudi Arabia, e-mail: balqahtani1@ksu.edu.sa
Pranay Goswami: School of Liberal Studies, Dr B. R. Ambedkar University Delhi, Delhi-110006, India, e-mail: pranaygoswami83@gmail.com

modeling the behavior of fluids under the influence of gravity. Emden-Fowler equations can also be applied to cosmology [8] to describe the behavior of certain types of dark matter, such as cold dark matter, which can be modeled as a polytropic fluid. The Emden-Fowler equation and its variants serve as mathematical models for various physical phenomena beyond astrophysics, including diffusion processes, population dynamics, and nonlinear wave propagation. In the context of chemical systems, similar mathematical models may arise to describe phenomena like diffusion-limited reactions in porous media.

The motivation behind studying Pantograph delay differential equations (PDDEs) [9] lies in their ability to capture and model systems where delays play a crucial role in the dynamics. These equations play a crucial role in a range of disciplines, encompassing physics [10], biology [11], and economics [12], as they can capture complex behaviors in systems with time delays. In control theory, systems with time delays are common in practical applications [13]. For example, in feedback control systems, there is often a finite time delay between the measurement of a system's state and the application of control action. PDDEs provide a mathematical framework to model and analyze the behavior of such systems, allowing engineers to design robust controllers that can handle delays effectively. Biological neural networks exhibit complex dynamics, including time delays in signal propagation between neurons. PDDEs are employed in computational neuroscience to model the dynamics of neural networks with delayed feedback and study phenomena like synchronization, oscillations, and information processing in the brain. PDDEs are used in macroeconomic modeling, financial markets analysis, and game theory to study the dynamics of economic systems with delays and understand phenomena like business cycles, market fluctuations, and policy impacts. In the context of delay differential equations (DDEs), the Pantograph concept is used to describe systems that involve time delays in such a way that they exhibit a particular form of stability and oscillatory behavior [14].

Within this article, we delve into the Emden-Fowler-type PDDEs of general order:

$$\frac{\mathrm{d}^{\varepsilon_1+\varepsilon_2}w(\nu)}{\mathrm{d}\nu^{\varepsilon_1+\varepsilon_2}} + \frac{\alpha}{\nu}\frac{\mathrm{d}^{\varepsilon_1+\varepsilon_2-1}w(\gamma\nu)}{\mathrm{d}\nu^{\varepsilon_1+\varepsilon_2-1}} + \frac{\beta}{\nu^2}\frac{\mathrm{d}^{\varepsilon_1+\varepsilon_2-2}w(\gamma\nu)}{\mathrm{d}\nu^{\varepsilon_1+\varepsilon_2-2}} + \ldots + s(\gamma\nu)g(w) = 0, \tag{2}$$

with initial conditions $w(0) = w_0$, $w'(0) = w_1$, $w''(0) = w_2, \ldots, w^{(\varepsilon_1+\varepsilon_2-1)}(0) = w_{\varepsilon_1+\varepsilon_2-1}$. Here γ, α, β are some suitable constants: $s(\nu)$ is an unknown function. Several pertinent papers discuss the notion of generalization, such as [15,16].

The inclusion of the delayed term in the equation reflects the system's sensitivity to its past values, introducing a notion of memory into the system's behavior. Analyzing and solving PDDEs can be challenging due to their non-standard form and the intricate interplay between delayed and non-delayed components. Researchers use a variety of mathematical techniques, such as Laplace transforms [17], numerical methods [18,19], and phase plane analysis, and Chebyshev polynomials [20] to understand the behavior of systems described by PDDEs. Srinivasa solved nonlinear variable DDEs using Laguerre wavelets in his paper [21].

Wavelets are mathematical functions used in various real-world applications [22] to analyze and process data in both one-dimensional and multi-dimensional forms. They have gained significant popularity in signal processing, data compression [23], and image analysis due to their ability to capture both high and low-frequency data components. In medical imaging, wavelets are used for tasks like image denoising [24], feature extraction [25], and image enhancement. In geophysics, wavelets are used to analyze seismic data [26]. They can help identify subsurface structures, locate natural resources, and assess the risk of seismic events. There are various types of wavelets, such as Haar wavelet [27,28], Morlet wavelet [29], Mexican hat wavelet [30], Daubechies wavelets, and Spline wavelets [31].

The Haar wavelet is fundamental and straightforward in signal processing and image compression. Formulated by the Hungarian mathematician Alfréd Haar during the early twentieth century, the Haar wavelet is a powerful tool for detecting edges in images [32]. It can detect sharp transitions in pixel values, which indicate edges and boundaries in images.

This study uses the Haar wavelet method to solve the PDDE. This study is organized as follows: Section 2 describes the Haar wavelet. Section 3 delves into the application and operation of the method in solving differential equations. Section 4 explores the convergence theorem and the rate of convergence. In Section 5, we discuss applications. Section 6 is dedicated to numerical simulations of the provided examples, accompanied by the compilation of error tables. Section 7, in turn, encompasses our concluding remarks and findings.

2 Haar wavelet

There are many wavelets. Haar wavelets are among the simplest types of wavelets, both conceptually and computationally. Their construction involves only basic binary operations and piecewise constant functions. Different wavelets have different advantages. It depends on certain contexts. For example, Haar wavelets have compact support. Unlike Haar wavelets, ultraspherical wavelets (described by Mulimani and Srinivasa in [33]) are not necessarily compactly supported; their support depends on the parameters of the ultraspherical polynomials but ultraspherical wavelets possess more flexibility in shaping the wavelet functions compared to Haar wavelets due to the adjustable parameters of ultraspherical polynomials. In scenarios where the detection and localization of sharp transitions are crucial, Haar wavelets may outperform ultraspherical wavelets, which may not be as sensitive to abrupt changes. Haar wavelet consists of a positive value and a negative value within a specific interval, and it is zero outside that interval. The Haar wavelet is orthogonal and has a compact support. Haar functions [34] over the interval $[0, 1)$ are defined as:

$$h_\mu(v) = \begin{cases} 1, & \xi_1 \le v < \xi_2, \\ -1, & \xi_2 \le v < \xi_3, \\ 0, & \text{otherwise}, \end{cases}$$

where

$$\xi_1 = \frac{l}{m}, \quad \xi_2 = \frac{2l+1}{2m}, \quad \xi_3 = \frac{l+1}{m}.$$

We define $m = 2^j$, $j = 0, 1, 2, \ldots J$, and $l = 0, 1, 2, \ldots m - 1$, where J is the maximum resolution, j represents the dilation parameter, and $\mu = m + l + 1$. For $\mu = 1$

$$h_1(v) = \begin{cases} 1, & v \in [0, 1], \\ 0, & \text{otherwise}. \end{cases}$$

$$h_2(v) = \begin{cases} 1, & v \in \left[0, \frac{1}{2}\right), \\ -1, & v \in \left[\frac{1}{2}, 1\right), \\ 0, & \text{otherwise}. \end{cases}$$

The Haar wavelet is orthogonal so

$$\int_0^1 h_\mu(v) h_b(v) \mathrm{d}v = \begin{cases} 2^{-j}; & \mu = b, \\ 0; & \mu \ne b. \end{cases}$$

For resolution, $J = 2$, Haar function matrix is given by

$$H_{8\times 8} = [h_1 \;\; h_2 \;\; h_3 \;\; h_4 \;\; h_5 \;\; h_6 \;\; h_7 \;\; h_8].$$

After substituting values

$$H_{8\times 8} = \begin{bmatrix} 1 & 1 & 1 & 1 & 1 & 1 & 1 & 1 \\ 1 & 1 & 1 & 1 & -1 & -1 & -1 & -1 \\ 1 & 1 & -1 & -1 & 0 & 0 & 0 & 0 \\ 0 & 0 & 0 & 0 & 1 & 1 & -1 & -1 \\ 1 & -1 & 0 & 0 & 0 & 0 & 0 & 0 \\ 0 & 0 & 1 & -1 & 0 & 0 & 0 & 0 \\ 0 & 0 & 0 & 0 & 1 & -1 & 0 & 0 \\ 0 & 0 & 0 & 0 & 0 & 0 & 1 & -1 \end{bmatrix}.$$

The integrals of the Haar function are defined as:

$$s_{\mu,1}(\nu) = \int_0^{\nu} h_\mu(\nu)\mathrm{d}\nu,$$

$$s_{\mu,2}(\nu) = \int_0^{\nu} s_{\mu,1}(\nu)\mathrm{d}\nu.$$

In general, we write

$$s_{\mu,\sigma}(\nu) = \begin{cases} 0, & \nu \in [0, \xi_1), \\ \frac{1}{\Gamma(\sigma+1)}(\nu - \xi_1)^\sigma, & \nu \in [\xi_1, \xi_2), \\ \frac{1}{\Gamma(\sigma+1)}[(\nu - \xi_1)^\sigma - 2(\nu - \xi_2)^\sigma], & \nu \in [\xi_2, \xi_3), \\ \frac{1}{\Gamma(\sigma+1)}[(\nu - \xi_1)^\sigma - 2(\nu - \xi_2)^\sigma + (\nu - \xi_3)^\sigma], & \nu \in [\xi_3, 1). \end{cases}$$

For resolution $J = 2$,

$$(S_1)_{8\times 8} = [s_{1,1} \quad s_{2,1} \quad s_{3,1} \quad s_{4,1} \quad s_{5,1} \quad s_{6,1} \quad s_{7,1} \quad s_{8,1}].$$

After substituting values

$$(S_1)_{8\times 8} = \begin{bmatrix} 0.0625 & 0.1875 & 0.3125 & 0.4375 & 0.5625 & 0.6875 & 0.8125 & 0.9375 \\ 0.0625 & 0.1875 & 0.3125 & 0.4375 & 0.4375 & 0.3125 & 0.1875 & 0.0625 \\ 0.0625 & 0.1875 & 0.1875 & 0.0625 & 0 & 0 & 0 & 0 \\ 0 & 0 & 0 & 0 & 0.0625 & 0.1875 & 0.1875 & 0.0625 \\ 0.0625 & 0.0625 & 0 & 0 & 0 & 0 & 0 & 0 \\ 0 & 0 & 0.0625 & 0.0625 & 0 & 0 & 0 & 0 \\ 0 & 0 & 0 & 0 & 0.0625 & 0.0625 & 0 & 0 \\ 0 & 0 & 0 & 0 & 0 & 0 & 0.0625 & 0.0625 \end{bmatrix}.$$

2.1 Function approximation

When dealing with a function $w(\nu)$ defined on the interval [0, 1], the approach involves approximating the function by employing Haar functions in the following manner:

$$w(\nu) = \sum_{\mu=1}^{\infty} c_\mu h_\mu,$$

where c_μ are the Haar coefficients.

3 Method

Let us consider the general order Emden-Fowler PDDE:

$$\frac{\mathrm{d}^{\varepsilon_1+\varepsilon_2} w(\nu)}{\mathrm{d}\nu^{\varepsilon_1+\varepsilon_2}} + \frac{\alpha}{\nu}\frac{\mathrm{d}^{\varepsilon_1+\varepsilon_2-1} w(\gamma\nu)}{\mathrm{d}\nu^{\varepsilon_1+\varepsilon_2-1}} + \frac{\beta}{\nu^2}\frac{\mathrm{d}^{\varepsilon_1+\varepsilon_2-2} w(\gamma\nu)}{\mathrm{d}\nu^{\varepsilon_1+\varepsilon_2-2}} + \ldots + s(\gamma\nu)g(w) = 0, \tag{3}$$

with initial conditions $w(0) = w_0,\ w'(0) = w_1,\ w''(0) = w_2, \ldots,\ w^{(\varepsilon_1+\varepsilon_2-1)}(0) = w_{\varepsilon_1+\varepsilon_2-1}$.

Now at first, we write

$$\frac{\mathrm{d}^{\varepsilon_1+\varepsilon_2} w(v)}{\mathrm{d}v^{\varepsilon_1+\varepsilon_2}} = \sum_{\mu=1}^{2T} c_\mu h_\mu(v). \tag{4}$$

We integrate this equation (4) and apply the initial conditions. We have

$$\frac{\mathrm{d}^{\varepsilon_1+\varepsilon_2-1} w(v)}{\mathrm{d}v^{\varepsilon_1+\varepsilon_2-1}} = \sum_{\mu=1}^{2T} c_\mu s_{\mu,1}(v) + w_{\varepsilon_1+\varepsilon_2-1}. \tag{5}$$

Repeatedly integrating and incorporating initial conditions, we obtain the following:

$$w(v) = \sum_{\mu=1}^{2T} c_\mu s_{\mu,\varepsilon_1+\varepsilon_2}(v) + \frac{v^{\varepsilon_1+\varepsilon_2-1}}{(\varepsilon_1+\varepsilon_2-1)!} w_{\varepsilon_1+\varepsilon_2-1} + \ldots + w_0. \tag{6}$$

After substituting all these equations into equation (3), equation (3) will be

$$\begin{aligned} &\sum_{\mu=1}^{2T} c_\mu h_\mu(v) + \sum_{\mu=1}^{2T} c_\mu s_{\mu,1}(\gamma v) + w_{\varepsilon_1+\varepsilon_2-1} + \ldots \sum_{\mu=1}^{2T} c_\mu s_{\mu,\varepsilon_1+\varepsilon_2}(\gamma v) \\ &+ \frac{(\gamma v)^{\varepsilon_1+\varepsilon_2-1}}{(\varepsilon_1+\varepsilon_2-1)!} w_{\varepsilon_1+\varepsilon_2-1} + \ldots + w_0 + s(\gamma v) g(w) = 0. \end{aligned} \tag{7}$$

In the next step, we collocate the points as:

$$v_\mu = \frac{\mu - 0.5}{2T}.$$

After collocating the points in equation (7), equation (7) will be

$$\begin{aligned} &\sum_{\mu=1}^{2T} c_\mu h_\mu(v_\mu) + \sum_{\mu=1}^{2T} c_\mu s_{\mu,1}(\gamma v_\mu) + w_{\varepsilon_1+\varepsilon_2-1} + \ldots \sum_{\mu=1}^{2T} c_\mu s_{\mu,\varepsilon_1+\varepsilon_2}(\gamma v_\mu) \\ &+ \frac{(\gamma v_\mu)^{\varepsilon_1+\varepsilon_2-1}}{(\varepsilon_1+\varepsilon_2-1)!} w_{\varepsilon_1+\varepsilon_2-1} + \ldots + w_0 + s(\gamma v_\mu) g(w) = 0. \end{aligned} \tag{8}$$

Now we have a system of equations of $2T \times 2T$. We utilize the Newton method for resolving this set of equations, resulting in the set of values of c_μ. After substituting the values of c_μ in equation (6) we have the numerical solution.

4 Error analysis and convergence

Lemma 4.1. [35] *Suppose* $w(v) \in L_2(\Re)$ *and has a bounded first derivative, that is,* $|w'(v)| \le Q, \ \forall v \in (0,1), Q > 0$, *and* $w(\mu) = \sum_{\mu=1}^{\infty} c_\mu h_\mu(v)$. *Then,* $|c_\mu| \le Q 2^{-(3k-2)/2}$.

Theorem 4.1. [35] *Consider a continuous function* $w(v) \in L_2(\Re)$ *within the interval (0, 1) that has a bounded first derivative. In this case, the error norm at the Jth level is determined by the following relationship*:

$$||E_J|| \le \sqrt{\frac{Q}{7}}\, C 2^{-(3/2)L}$$

$|w'(v)| \le Q, \ \forall v \in (0,1), Q > 0$, *and* $N = 2^k$, *where J represents the highest resolution.*

The demonstration is simple and direct [35].

Table 1: Rate of convergence for Examples

Resolution (J)	3	4	5	6
Example 1 ($R_C(J)$)	1.897402	1.949923	1.987721	1.992677
Example 2 ($R_C(J)$)	1.481526	1.731874	1.863017	1.9307027
Example 3 ($R_C(J)$)	3.110294	1.306188	1.907927	2.005272

4.1 Error analysis

The error is determined as follows:

$$L_\infty = \text{Max.}|w_\mu^{\text{exact}} - w_\mu^{\text{approx.}}|,$$

where w_μ^{exact} and $w_\mu^{\text{approx.}}$ represent the exact and estimated solutions at the μth point.

4.2 Rate of convergence

The definition of the convergence rate is as follows:

$$R_C(J) = \frac{\log[E_C(J/2)/E_C(J)]}{\log 2},$$

where $E_C(J)$ denotes the maximum absolute error across J collocation points.

The rate of convergence of a numerical method refers to how quickly the method converges to the true solution or how fast the error decreases with each iteration. Table 1 shows the rate of convergence for Example 1, Example 2, and Example 3.

5 Applications

5.1 Application 1

Let us consider the fourth-order Emden-Fowler PDE:

$$\frac{\mathrm{d}^4 w(v)}{\mathrm{d}v^4} + \frac{4}{v}\frac{\mathrm{d}^3 w(v/2)}{\mathrm{d}v^3} + e^{w(v/2)} = Z(v), \tag{9}$$

where

$$Z(v) = \left(\frac{1}{1+v^4}\right)^4 [24 - 744v^4 + 744v^8 - 24v^{12}] + \left(\frac{1}{16+v^4}\right)^3 [196{,}608 - 49{,}152v^4 + 256v^8] + \left(\frac{16+v^4}{16}\right)e,$$

with initial conditions: $w(0) = 1,\ w'(0) = 0,\ w''(0) = 0,\ w'''(0) = 0$.

$w(v) = 1 + \log(1 + v^4)$ represents the exact solution of (9).

Now we apply the method. Consider

$$\frac{\mathrm{d}^4 w(v)}{\mathrm{d}v^4} = \sum_{\mu=1}^{2T} c_\mu h_\mu(v). \tag{10}$$

After performing the integration of (10) and implementing the initial condition, we have

$$\frac{\mathrm{d}^3 w(v)}{\mathrm{d}v^3} = \sum_{\mu=1}^{2T} c_\mu s_{\mu,1}(v) \tag{11}$$

and

$$\frac{\mathrm{d}^3 w(v/2)}{\mathrm{d}v^3} = \sum_{\mu=1}^{2T} c_\mu s_{\mu,1}(v/2). \tag{12}$$

Integrating equation (11) again and again and applying initial conditions, we have

$$w(v) = 1 + \sum_{\mu=1}^{2T} c_\mu s_{\mu,4}(v) \tag{13}$$

and

$$w(v/2) = 1 + \sum_{\mu=1}^{2T} c_\mu s_{\mu,4}(v/2). \tag{14}$$

After substituting equations (10), (12), and (14) into equation (9), we have a system of equations after the collocation of points:

$$\sum_{\mu=1}^{2T} c_\mu h_\mu(v_\mu) + \frac{4}{v_\mu}\left(\sum_{\mu=1}^{2T} c_\mu s_{\mu,1}(v_\mu/2)\right) + e^{1+\sum_{\mu=1}^{2T} c_\mu s_{\mu,4}(v_\mu/2)} - Z(v_\mu) = 0. \tag{15}$$

The Newton method is used to resolve this equation system and acquire the Haar coefficients denoted as c_μ. Subsequently, substituting these coefficients into equation (13) yields the estimated solution.

5.2 Application 2

Let us consider fifth-order Emden-Fowler PDDE:

$$\frac{\mathrm{d}^5 w(v)}{\mathrm{d}v^5} + \frac{4}{v}\frac{\mathrm{d}^4 w(v/2)}{\mathrm{d}v^4} + \frac{2}{v^2}\frac{\mathrm{d}^3 w(v/2)}{\mathrm{d}v^3} - \frac{5w(v/2)}{16{,}384}F(v) = G(v), \tag{16}$$

where

$$F(v) = 884{,}736 + 506{,}880v^5 + 19{,}400\,v^{10} + 125v^{15},$$

$$G(v) = 5e^{v^5}[24 + 3{,}000v^5 + 9{,}000v^{10} + 5{,}000\,v^{15} + 625v^{20}],$$

with initial conditions $w(0) = 1,\ w'(0) = 0,\ w''(0) = 0,\ w'''(0) = 0,\ w''''(0) = 0$.

$w(v) = e^{v^5}$ represents the exact solution of (16).

Now we apply the method. Consider

$$\frac{\mathrm{d}^5 w(v)}{\mathrm{d}v^5} = \sum_{\mu=1}^{2T} c_\mu h_\mu(v). \tag{17}$$

Integrating equation (17) again and again and applying initial conditions, we have

$$w(v) = 1 + \sum_{\mu=1}^{2T} c_\mu s_{\mu,5}(v) \tag{18}$$

and

$$w(v/2) = 1 + \sum_{\mu=1}^{2T} c_\mu s_{\mu,5}(v/2). \tag{19}$$

After substituting these equations into equation (16), we have a system of equations after collocation of points:

$$\sum_{\mu=1}^{2T} c_\mu h_\mu(\nu_\mu) + \frac{4}{\nu_\mu}\left(\sum_{\mu=1}^{2T} c_\mu s_{\mu,1}(\nu_\mu/2)\right) + \frac{2}{\nu_\mu^2}\left(\sum_{\mu=1}^{2T} c_\mu s_{\mu,2}(\nu_\mu/2)\right) - \frac{5(1+\sum_{\mu=1}^{2T} c_\mu s_{\mu,5}(\nu_\mu/2))}{16{,}384}F(\nu_\mu) - G(\nu_\mu) = 0. \tag{20}$$

The Newton method is used to resolve this equation system and acquire the Haar coefficients denoted as c_μ. Subsequently, substituting these coefficients into equation (18) yields the estimated solution.

5.3 Application 3

Consider the sixth-order Emden-Fowler multi-term PDDE:

$$\frac{\mathrm{d}^6 w(\nu)}{\mathrm{d}\nu^6} + \frac{1}{\nu}\frac{\mathrm{d}^5 w(\nu/2)}{\mathrm{d}\nu^5} + (w(\nu/2))^7\left[360 - 210\nu^2 - \frac{105}{2}\nu^4 + \frac{45}{8}\nu^6\right] - 720(w(\nu))^7[-1 + 21\nu^2 - 35\nu^4 + 7\nu^6] = 0, \tag{21}$$

with initial conditions $w(0) = 1$, $w'(0) = 0$, $w''(0) = -2$, $w'''(0) = 0$, $w''''(0) = 24$, $w''''(0) = 0$.

$w(\nu) = \frac{1}{1+\nu^2}$ represents the exact solution of (21).

Now we apply the method. Consider

$$\frac{\mathrm{d}^6 w(\nu)}{\mathrm{d}\nu^6} = \sum_{\mu=1}^{2T} c_\mu h_\mu(\nu). \tag{22}$$

Integrating equation (22) again and again and applying initial conditions, we have

$$w(\nu) = 1 - \nu^2 + \nu^4 + \sum_{\mu=1}^{2T} c_\mu s_{\mu,6}(\nu) \tag{23}$$

and

$$w(\nu/2) = 1 - (\nu/2)^2 + (\nu/2)^4 + \sum_{\mu=1}^{2T} c_\mu s_{\mu,6}(\nu/2). \tag{24}$$

After substituting these equations into equation (21), we have a system of equations after collocation of points:

$$\begin{aligned}&\sum_{\mu=1}^{2T} c_\mu h_\mu(\nu_\mu) + \frac{1}{\nu_\mu}\left(\sum_{\mu=1}^{2T} c_\mu s_{\mu,1}(\nu_\mu/2)\right)\\ &+ \left(1 - (\nu_\mu/2)^2 + (\nu_\mu/2)^4 + \sum_{\mu=1}^{2T} c_\mu s_{\mu,6}(\nu_\mu/2)\right)^7\left[360 - 210{\nu_\mu}^2 - \frac{105}{2}{\nu_\mu}^4 + \frac{45}{8}{\nu_\mu}^6\right]\\ &- 720\left(1 - {\nu_\mu}^2 + {\nu_\mu}^4 + \sum_{\mu=1}^{2T} c_\mu s_{\mu,6}(\nu_\mu)\right)^7[-1 + 21{\nu_\mu}^2 - 35{\nu_\mu}^4 + 7{\nu_\mu}^6] = 0.\end{aligned} \tag{25}$$

The Newton method is used to resolve this equation system and acquire the Haar coefficients denoted as c_μ. Subsequently, substituting these coefficients into equation (23) yields the Haar solution.

5.4 Application 4

Consider the sixth-order Emden-Fowler multi-term PDDE:

$$\frac{\mathrm{d}^6 w(\nu)}{\mathrm{d}\nu^6} + \frac{12}{\nu}\frac{\mathrm{d}^5 w(\nu/2)}{\mathrm{d}\nu^5} + \frac{36}{\nu^2}\frac{\mathrm{d}^4 w(\nu/2)}{\mathrm{d}\nu^4} + \frac{24}{\nu^3}\frac{\mathrm{d}^3 w(\nu/2)}{\mathrm{d}\nu^3} - 8{,}640 = 0, \tag{26}$$

with initial conditions $w(0) = 1$, $w'(0) = 0$, $w''(0) = 0$, $w'''(0) = 0$, $w''''(0) = 0$, $w'''''(0) = 0$.

$w(\nu) = 1 + \nu^6$ represents the exact solution of (26).

Now we apply the method. Consider

$$\frac{\mathrm{d}^6 w(\nu)}{\mathrm{d}\nu^6} = \sum_{\mu=1}^{2T} c_\mu h_\mu(\nu). \tag{27}$$

Integrating equation (27) again and again and applying initial conditions, we have

$$w(\nu) = 1 + \sum_{\mu=1}^{2T} c_\mu s_{\mu,6}(\nu) \tag{28}$$

and

$$w(\nu/2) = 1 + \sum_{\mu=1}^{2T} c_\mu s_{\mu,6}(\nu/2). \tag{29}$$

After substituting these equations into equation (26), we have a system of equations after collocation of points:

$$\sum_{\mu=1}^{2T} c_\mu h_\mu(\nu_\mu) + \frac{12}{\nu_\mu}\left(\sum_{\mu=1}^{2T} c_\mu s_{\mu,1}(\nu_\mu/2)\right) + \frac{36}{\nu_\mu^2}\left(\sum_{\mu=1}^{2T} c_\mu s_{\mu,2}(\nu_\mu/2)\right) + \frac{24}{\nu_\mu^3}\left(\sum_{\mu=1}^{2T} c_\mu s_{\mu,3}(\nu_\mu/2)\right) - 8{,}640 = 0. \tag{30}$$

The Newton method is used to resolve this equation system and acquire the Haar coefficients denoted as c_μ. Subsequently, substituting these coefficients into equation (28) yields the Haar solution.

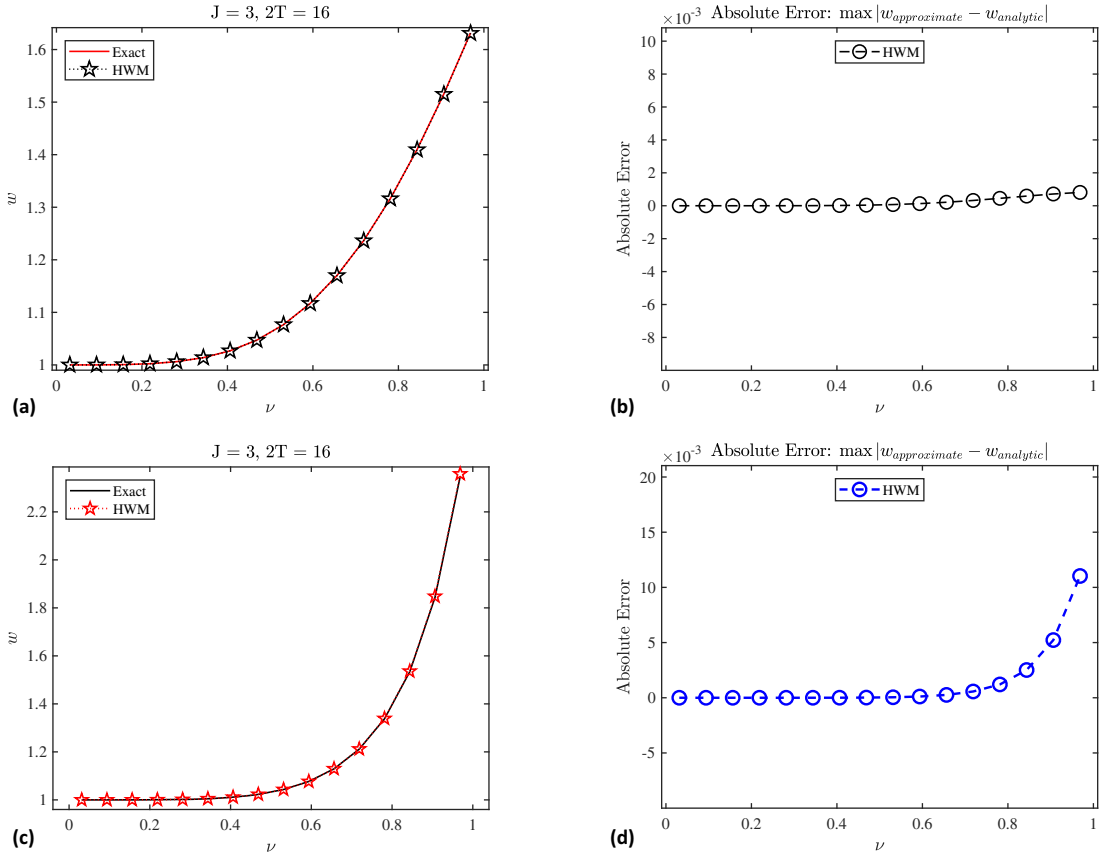

Figure 1: Graphical demonstration of Application 1 and Application 2. (a) Comparison of exact solution with Haar wavelet method (HWM) solution for Application 1 when $J = 3$, (b) absolute error of Application 1 when $J = 3$, (c) comparison of exact solution with HWM solution for Application 2 when $J = 3$, and (d) absolute error of Application 2 when $J = 3$.

6 Numerical simulation

Figure 1 depicts the error and comparison between the exact solution and the Haar wavelet solution for Example 1 and Example 2. Figures 2 and 3 depict the error and comparison between the exact and Haar wavelet solution for example 2 and example 3 respectively. Tables 2–5 illustrate the comparison between exact and Haar solution at various values of ν. Tables 6–9 give the maximum absolute error for different resolutions. These tables also provide the CPU time, indicating that this method exhibits a notable speed.

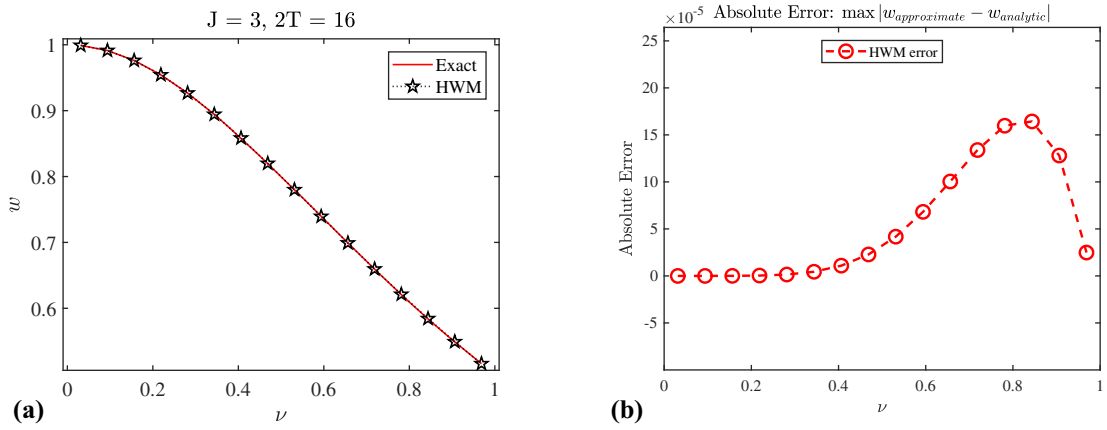

Figure 2: Graphical demonstration of Application 3. (a) Comparison of exact solution with HWM solution for Application 3 when $J = 3$ and (b) absolute error of Application 3 when $J = 3$.

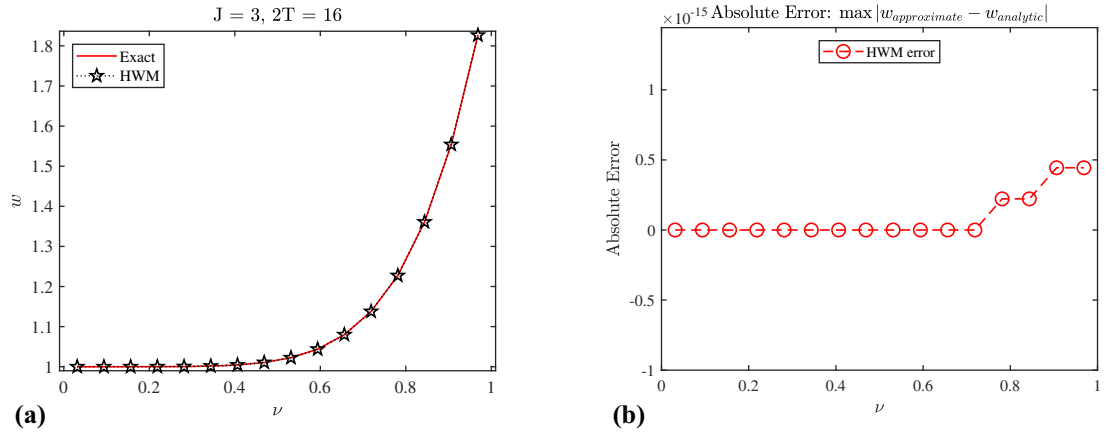

Figure 3: Numerical simulation of Example 4. (a) Comparison of exact solution with HWM solution for Application 4 when $J = 3$ and (b) absolute error of Application 4 when $J = 3$.

Table 2: Comparison of Haar wavelet solution with exact solution for Application 1 at $J = 3$

v	HWM	Exact	Error
0.1	1.00009999	1.00009999	1.553×10^{-9}
0.2	1.00159844	1.00159872	2.715×10^{-7}
0.3	1.00806459	1.00806737	2.775×10^{-6}
0.4	1.02526313	1.02527780	1.467×10^{-5}
0.5	1.06057291	1.06062462	5.171×10^{-5}
0.6	1.12172689	1.12186358	1.366×10^{-4}
0.7	1.21490555	1.21519202	2.864×10^{-4}
0.8	1.34281450	1.34330597	4.914×10^{-4}
0.9	1.50376271	1.50446544	7.027×10^{-4}

Table 3: Comparison of Haar wavelet solution with exact solution for Application 2 at $J = 3$

v	HWM	Exact	Error
0.1	1.00001000	1.00001000	2.979×10^{-11}
0.2	1.00032007	1.00032005	1.940×10^{-8}
0.3	1.00243341	1.00243295	4.559×10^{-7}
0.4	1.01029712	1.01029260	4.512×10^{-6}
0.5	1.03177062	1.03174340	2.721×10^{-5}
0.6	1.08098489	1.08086322	1.216×10^{-4}
0.7	1.18347043	1.18301941	4.510×10^{-4}
0.8	1.38925012	1.38774482	1.505×10^{-3}
0.9	1.80972919	1.80487258	4.856×10^{-3}

Table 4: Comparison of Haar wavelet solution with exact solution for Application 3 at $J = 3$

v	HWM	Exact	Error
0.1	0.99009901	0.99009900	9.544×10^{-9}
0.2	0.96153870	0.96153846	2.401×10^{-7}
0.3	0.91743329	0.91743119	2.101×10^{-6}
0.4	0.86207902	0.86206896	1.005×10^{-5}
0.5	0.80003134	0.80000000	3.134×10^{-5}
0.6	0.73536528	0.73529411	7.116×10^{-5}
0.7	0.67126510	0.67114093	1.241×10^{-4}
0.8	0.60992023	0.60975609	1.641×10^{-4}
0.9	0.55262038	0.55248618	1.341×10^{-4}

Table 5: Comparison of Haar wavelet solution with exact solution for Application 4 at $J = 3$

v	HWM	Exact	Error
0.1	1.00000100	1.00000100	0
0.2	1.00006400	1.00006400	0
0.3	1.00072900	1.00072900	0
0.4	1.00409600	1.00409600	0
0.5	1.01562500	1.01562500	0
0.6	1.04665600	1.04665600	0
0.7	1.11764900	1.11764900	0
0.8	1.26214400	1.26214400	0
0.9	1.53144100	1.53144100	0

Table 6: Maximum absolute error of Application 1

Resolution	System of equations	HWM error	CPU time in seconds
$J = 3$	16×16	8.100×10^{-4}	1.124490
$J = 4$	32×32	2.090×10^{-4}	1.338281
$J = 5$	64×64	5.286×10^{-5}	1.728761
$J = 6$	128×128	1.328×10^{-5}	3.793212
$J = 7$	256×256	3.346×10^{-6}	15.148980
$J = 8$	512×512	8.562×10^{-7}	99.325444

Table 7: Maximum absolute error of Application 2

Resolution	System of equations	HWM error	CPU time in seconds
$J = 3$	16×16	1.103×10^{2}	1.162713
$J = 4$	32×32	3.321×10^{3}	1.380484
$J = 5$	64×64	9.131×10^{4}	2.009864
$J = 6$	128×128	2.395×10^{4}	5.376645
$J = 7$	256×256	6.134×10^{5}	25.112066
$J = 8$	512×512	1.552×10^{5}	167.294925

Table 8: Maximum absolute error of Application 3

Resolution	System of equations	HWM error	CPU time in seconds
$J = 3$	16×16	1.643×10^{-4}	1.294916
$J = 4$	32×32	6.644×10^{-5}	1.650631
$J = 5$	64×64	1.770×10^{-5}	2.602486
$J = 6$	128×128	4.410×10^{-6}	7.337785
$J = 7$	256×256	1.099×10^{-6}	35.188070
$J = 8$	512×512	2.748×10^{-7}	236.130223

Table 9: Maximum absolute error of Application 4

Resolution	System of equations	HWM error	CPU time in seconds
$J = 3$	16×16	4.4409×10^{-16}	1.284342
$J = 4$	32×32	1.3323×10^{-15}	1.769604
$J = 5$	64×64	4.4409×10^{-16}	3.876561
$J = 6$	128×128	3.1086×10^{-15}	14.472351
$J = 7$	256×256	3.9968×10^{-15}	165.167635

7 Conclusion

We investigate the use of the Haar wavelet method as a valuable numerical technique to solve differential equations and perform various mathematical and scientific calculations in this study. We have also delved into the fascinating and challenging realm of PDDE, exploring their mathematical properties, analytical solutions, and numerical approximations. The complexity of these equations, combined with their wide-ranging

applications, makes them a captivating subject for mathematicians, scientists, and engineers. The Haar wavelet collocation method leverages the simplicity and piecewise constant nature of Haar wavelets to approximate solutions to differential equations efficiently and accurately. It excels at handling problems with discontinuities and sharp changes in the solution, making it a suitable choice for various applications in science and engineering. In this study, we have demonstrated the method's effectiveness.

In conclusion, the Haar wavelet collocation method is a valuable numerical analysis tool. Its simplicity, ability to handle discontinuities, and potential for accurate approximations make it a compelling choice for a broad spectrum of issues. The Haar wavelet collocation method, while not without its limitations, offers a promising path toward solving complex mathematical and scientific challenges. Its efficiency and accuracy in approximating solutions make it a valuable addition to the numerical methods available to researchers and practitioners.

Funding information: This work was supported and funded by the Deanship of Scientific Research at Imam Mohammad Ibn Saud Islamic University (IMSIU) (grant number IMSIU-RP23028).

Author contributions: P.G. spearheaded the investigation and coordinated the necessary literature. A.K. composed the manuscript, interpreted the findings, performed all numerical calculations, and generated the graphs. K.S.A. and B.S.A. compiled the data for tables, crafted the study site map, and formatted the final document. All authors have reviewed and consented to the published version of the manuscript.

Conflict of interest: The article presented is declared to be free from any conflicts of interest by the researchers.

Ethical approval: The conducted research is not related to either human or animals use.

Data availability statement: Not applicable.

References

[1] R. Emden, *Anwendungen der Mechanischen Wärmetheorie auf Kosmologische und Meteorologische Problem*, BG Teubner, Leipzig, 1907.
[2] R. H. Fowler, *Emden's equation: The solutions of Emden's and similar differential equations*, Monthly Notices R Astronom Soc. **91** (1930), 63, https://adsabs.harvard.edu/full/1930mnras..91...63f.
[3] S. Chandrasekhar and S. Chandrasekhar, *An Introduction to the Study of Stellar Structure*, Courier Corporation, United States, 1957.
[4] R. Kippenhahn, A. Weigert, and A. Weiss, *Stellar Structure and Evolution*, Springer-verlag, Berlin, 1990, DOI: https://doi.org/10.1007/978-3-642-30304-3.
[5] M. V. Penston, *Dynamics of self-gravitating gaseous spheres-II. Collapses of gas spheres with cooling and the behavior of polytropic gas spheres*, Mon. Not. R. Astron. Soc. **145** (1969), 457, DOI: https://doi.org/10.1093/mnras/145.4.457.
[6] M. J. Thompson, *An Introduction to Astrophysical Fluid Dynamics*, World Scientific, Singapore, Jan 17, 2006, DOI: https://doi.org/10.1142/p418.
[7] Z. Zhang, *The asymptotic behavior of the unique solution for the singular Lane-Emden-Fowler equation*, J Math Anal Appl. **312** (2005), no. 1, 33–43, DOI: https://doi.org/10.1016/j.jmaa.2005.03.023.
[8] K. Moodley, *Aspects of spherically symmetric cosmological models*, Ph.D. Dissertion, Natal University, 1998, http://hdl.handle.net/10413/3909.
[9] H. Jafari, M. Mahmoudi, and M. H. Noori Skandari, *A new numerical method to solve pantograph delay differential equations with convergence analysis*, Adv. Difference Equations **2021** (2021), no. 1, 129, DOI: https://doi.org/10.1186/s13662-021-03293-0.
[10] T. Griebel, *The Pantograph Equation in Quantum Calculus*, Missouri University of Science and Technology, 2017, https://api.semanticscholar.org/CorpusID:125111622.
[11] B. Van Brunt, A. A. Zaidi, and T. Lynch, *Cell division and the pantograph equation*, ESAIM: Proc. Surveys **62** (2018), 158–167, DOI: https://doi.org/10.1051/proc/201862158.
[12] M. A. Eissa and M. Elsayed, *Improve stock price model-based stochastic pantograph differential equation*, Symmetry **14** (Jul 1, 2022), no. 7, 1358, DOI: https://doi.org/10.3390/sym14071358.
[13] Y. C. Lin, N. C. Shieh, and V. T. Liu, *Optimal control for rail vehicle pantograph systems with actuator delays*, IET Control Theory Appl. **9** (2015), no. 13, 1917–1926, DOI: https://doi.org/10.1049/iet-cta.2014.1263.

[14] K. Guan, *Oscillation of solutions of a neutral pantograph equation with impulsive perturbations*, Turkish J Math. **37** (2013), no. 3, 455–465, DOI: https://doi.org/10.3906/mat-1111-38.
[15] H. M. Srivastava, R. S. Dubey, and M. Jain, *A study of the fractional-order mathematical model of diabetes and its resulting complications*, Math. Methods Appl. Sci. **42** (2019), no. 13, 4570–4583, DOI: https://doi.org/10.1002/mma.5681.
[16] S. S. Alzaid, B. S. Alkahtani, S. Sharma, and R.S. Dubey, *Numerical solution of fractional model of HIV-1 infection in the framework of different fractional derivatives*, J. Funct. Spaces. **2021** (2021), 6642957, DOI: https://doi.org/10.1155/2021/6642957.
[17] R. Alrebdi and H. K. Al-Jeaid, *Accurate solution for the Pantograph delay differential equation via Laplace transform*, Mathematics **11** (2023), no. 9, 2031, DOI: https://doi.org/10.3390/math11092031.
[18] J. Hajishafieiha and S. Abbasbandy, *Numerical approach for solving the fractional pantograph delay differential equations*, Complexity **2022** (2022), no. 1, 4134892, DOI: https://doi.org/10.1155/2022/4134892.
[19] D. Li and M. Z. Liu, *Runge-Kutta methods for the multi-pantograph delay equation*, Appl. Math. Comput. **163** (2005), no. 1, 383–395, DOI: https://doi.org/10.1016/j.amc.2004.02.013.
[20] S. Sedaghat, Y. Ordokhani, and M. Dehghan, *Numerical solution of the delay differential equations of pantograph type via Chebyshev polynomials*, Commun. Nonlinear Sci. Numer. Simul. **17** (2012), no. 12, 4815–4830, DOI: https://doi.org/10.1016/j.cnsns.2012.05.009.
[21] K. Srinivasa and R. A. Mundewadi, *Wavelets approach for the solution of nonlinear variable delay differential equations*, Int. J. Math. Comput. Eng. **1** (2023), no. 2, 139–148, DOI: https://doi.org/10.2478/ijmce-2023-0011.
[22] I. Meyer, *Wavelets and Applications*, Masson, Paris, 1992, p. 31, https://jqichina.files.wordpress.com/2012/02/e3808awaveletse28094algorithms-applicationse3808byves-meyere79d80robert-d-ryane8af911993.pdf.
[23] W. R. Zettler, J. C. Huffman, and D. C. Linden, *Application of compactly supported wavelets to image compression*, Image Process Algorithms Tech. **1244** (1990), 150–160, SPIE, DOI: https://doi.org/10.1117/12.19505.
[24] S. D. Ruikar and D. D. Doye, *Wavelet based image denoising technique*, Int. J. Adv. Comput. Sci. Appl. **2** (2011), no. 3, DOI: https://dx.doi.org/10.14569/IJACSA.2011.020309.
[25] B. H. Chen, X. Z. Wang, S. H. Yang, and C. McGreavy, *Application of wavelets and neural networks to diagnostic system development, 1, Feature Extraction*, Comput. Chem. Eng. **23** (1999), no. 7, 899–906, DOI: https://doi.org/10.1016/S0098-1354(99)00258-6.
[26] X. G. Miao and W. M. Moon, *Application of wavelet transform in reflection seismic data analysis*, Geosci. J. **3** (1999), 171–179, DOI: https://doi.org/10.1007/BF02910273.
[27] C. K. Chui, *An Introduction to Wavelets*, Academic Press, London, 1992, DOI: http://dx.doi.org/10.2307/2153134.
[28] C. F. Chen and C. H. Hsiao, *Haar wavelet method for solving lumped and distributed-parameter systems*, IEE Proc. Control Theory Appl. **144** (1997), no. 1, 87–94, DOI: https://doi.org/10.1049/ip-cta:19970702.
[29] R. Büssow, *An algorithm for the continuous Morlet wavelet transform*, Mech. Syst. Signal Process **21** (2007), no. 8, 2970–2979, DOI: https://doi.org/10.1016/j.ymssp.2007.06.001.
[30] Z. Zhou and H. Adeli, *Time-frequency signal analysis of earthquake records using Mexican hat wavelets*, Comput. Aided Civil Infrastruct. Eng. **18** (2003), no. 5, 379–389, DOI: https://doi.org/10.1111/1467-8667.t01-1-00315.
[31] C K. Chui and J. Z. Wang, *On compactly supported spline wavelets and a duality principle*, Trans. Amer. Math. Soc. **330** (1992), no. 2, 903–915, DOI: https://doi.org/10.2307/2153941.
[32] J. Mashford, M. Rahilly, B. Lane, D. Marney, and S. Burn, *Edge detection in pipe images using classification of Haar wavelet transforms*, Appl. Artif. Intelligence. **28** (2014), no. 7, 675–689, DOI: https://doi.org/10.1080/08839514.2014.927689.
[33] M. Mulimani and K. Srinivasa, *A novel approach for Benjamin-Bona-Mahony equation via ultraspherical wavelets collocation method*, Int. J. Math. Comput. Eng. (2024), DOI: https://doi.org/10.2478/ijmce-2024-0014.
[34] S. Arbabi, A. Nazari, and M. T. Darvishi, *A two-dimensional Haar wavelets method for solving systems of PDEs*, Appl. Math. Comput. **292** (2017), 33–46, DOI: https://doi.org/10.1016/j.amc.2016.07.032.
[35] S. S. Ray, *On Haar wavelet operational matrix of general order and its application for the numerical solution of fractional Bagley Torvik equation*, Appl. Math. Comput. **218** (2012), no. 9, 5239–5248, DOI: https://doi.org/10.1016/j.amc.2011.11.007.